Published in Journal of Organometallic Chemistry 692, issue 17, 3664-3675, 2007
which should be used for any reference to this work

Mono and dinuclear rhodium, iridium and ruthenium complexes containing chelating 2,2′-bipyrimidine ligands: Synthesis, molecular structure, electrochemistry and catalytic properties

Padavattan Govindaswamy [a], Jérôme Canivet [a], Bruno Therrien [a], Georg Süss-Fink [a,*], Petr Štěpnička [b,*], Jiří Ludvík [c]

[a] *Institut de Chimie, Université de Neuchâtel, Case postale 158, CH-2009 Neuchâtel, Switzerland*
[b] *Charles University, Faculty of Natural Science, Department of Inorganic Chemistry, Hlavova 2030, CZ-12840 Prague 2, Czech Republic*
[c] *J. Heyrovský Institute of Physical Chemistry, Academy of Sciences of the Czech Republic, Dolejškova 3, CZ-18223 Prague, Czech Republic*

Abstract

The mononuclear cations $[(\eta^5\text{-}C_5Me_5)RhCl(bpym)]^+$ (**1**), $[(\eta^5\text{-}C_5Me_5)IrCl(bpym)]^+$ (**2**), $[(\eta^6\text{-}p\text{-}Pr^iC_6H_4Me)RuCl(bpym)]^+$ (**3**) and $[(\eta^6\text{-}C_6Me_6)RuCl(bpym)]^+$ (**4**) as well as the dinuclear dications $[\{(\eta^5\text{-}C_5Me_5)RhCl\}_2(bpym)]^{2+}$ (**5**), $[\{(\eta^5\text{-}C_5Me_5)IrCl\}_2(bpym)]^{2+}$ (**6**), $[\{(\eta^6\text{-}p\text{-}Pr^iC_6H_4Me)RuCl\}_2(bpym)]^{2+}$ (**7**) and $[\{(\eta^6\text{-}C_6Me_6)RuCl\}_2(bpym)]^{2+}$ (**8**) have been synthesised from 2,2′-bipyrimidine (bpym) and the corresponding chloro complexes $[(\eta^5\text{-}C_5Me_5)RhCl_2]_2$, $[(\eta^5\text{-}C_5Me_5)IrCl_2]_2$, $[(\eta^6\text{-}Pr^iC_6H_4Me)RuCl_2]_2$ and $[(\eta^6\text{-}C_6Me_6)RuCl_2]_2$, respectively. The X-ray crystal structure analyses of [**3**][PF_6], [**5**][PF_6]$_2$, [**6**][CF_3SO_3]$_2$ and [**7**][PF_6]$_2$ reveal a typical piano-stool geometry around the metal centres; in the dinuclear complexes the chloro ligands attached to the two metal centres are found to be, with respect to each other, *cis* oriented for **5** and **6** but *trans* for **7**. The electrochemical behaviour of **1**–**8** has been studied by voltammetric methods. In addition, the catalytic potential of **1**–**8** for transfer hydrogenation reactions in aqueous solution has been evaluated: All complexes catalyse the reaction of acetophenone with formic acid to give phenylethanol and carbon dioxide. For both the mononuclear and dinuclear series the best results were obtained (50 °C, pH 4) with rhodium complexes, giving turnover frequencies of 10.5 h^{-1} for **1** and 19 h^{-1} for **5**.

Keywords: Arene ligands; Dinuclear complexes; Transfer hydrogenation; N ligands; Electrochemistry

1. Introduction

Water-soluble organometallic complexes attract continuously growing interest for applications in catalysis because of environmentally friendly processing, simple product separation and pH dependent selectivity in aqueous media [1,2].

Recent reports deal with cationic water-soluble complexes such as $[(\eta^5\text{-}C_5Me_5)Ir(bpy)(H_2O)]^{2+}$ [3], $[(\eta^6\text{-}C_6Me_6)Ru(bpy)(H_2O)]^{2+}$ [4] and $[(\eta^5\text{-}C_5Me_5)Rh(bpy)Cl]^+$ [5] (bpy = 2,2′-bipyridine), which have been found to act as catalyst precursors for pH-dependent transfer hydrogenation of water-soluble and insoluble ketones with formate as a hydrogen source in water. We have shown that the cationic arene ruthenium complex $[(\eta^6\text{-}C_6Me_6)Ru(phen)Cl]^+$ (phen = 1,10-phenanthroline) catalyses the transfer hydrogenation of acetophenone with formic acid in aqueous solution to give phenylethanol and carbon dioxide [6]. A catalytic cycle was proposed based on our results coupled with mechanistic studies by Ogo et al. [4].

* Corresponding authors.
E-mail addresses: georg.suess-fink@unine.ch (G. Süss-Fink), stepnic@natur.cuni.cz (P. Štěpnička).

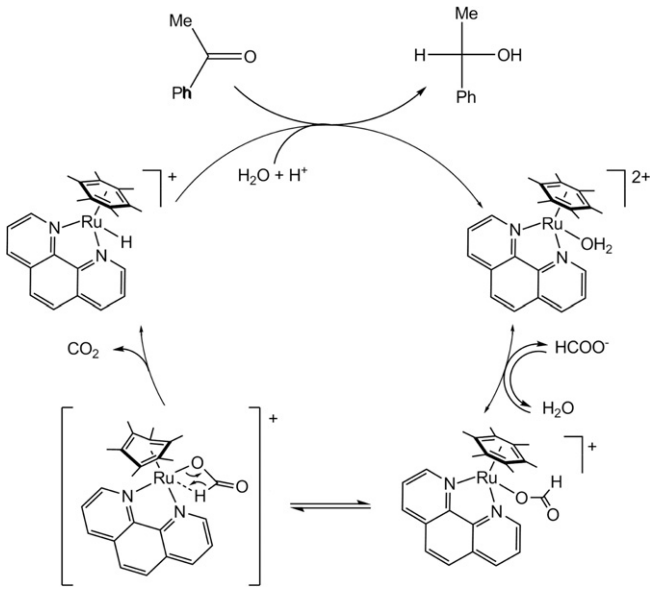

In the case of the 2,2′-bipyridine analogues, Ogo et al. succeeded in the isolation of the hydrido [7,8] and the formato intermediates [4]. In order to gain a deeper insight into this reaction, particularly as far as the catalytic activity of different metals is concerned, we prepared two series of mono and dinuclear pentamethylcyclopentadienyl rhodium(III), iridium(III) and arene ruthenium(II) complexes containing 2,2′-bipyrimidine as terminal or bridging chelate ligand. The catalytic activity of these complexes for the transfer hydrogenation of aromatic ketones to give the corresponding secondary alcohol with sodium formate as the hydrogen donor in aqueous solution is reported. We also present the electrochemical behaviour of the compounds and the single-crystal X-ray structure analysis of some representatives.

2. Results and discussion

*2.1. Synthesis of the mononuclear complexes **1**–**4** as hexafluorophosphate salts*

The pentamethylcyclopentadienyl or arene complexes $[(\eta^5\text{-}C_5Me_5)MCl_2]_2$ (M = Rh, Ir) and $[(\eta^6\text{-arene})RuCl_2]_2$ (arene = *p*-Pr^{i}C$_6$H$_4$Me, C$_6$Me$_6$) react with 2 equiv. of 2,2′-bipyrimidine (bpym) in methanol to form the cationic pentamethylcyclopentadienyl complexes $[(\eta^5\text{-}C_5Me_5)RhCl(bpym)]^+$ (**1**), $[(\eta^5\text{-}C_5Me_5)IrCl(bpym)]^+$ (**2**), as well as the cationic arene ruthenium complexes $[(\eta^6\text{-}p\text{-}Pr^iC_6H_4Me)RuCl(bpym)]^+$ (**3**) and $[(\eta^6\text{-}C_6Me_6)RuCl(bpym)]^+$ (**4**), which are isolated as their hexafluorophosphate salts (Scheme 1). The cationic complexes **1**–**4** are orange–red, resulting as non-hygroscopic, air-stable, shiny crystalline solids. They are sparingly soluble in methanol and chloroform, but well soluble in dichloromethane, acetone and acetonitrile. All compounds were characterised by elemental analysis, ^{1}H NMR, IR and mass spectroscopy.

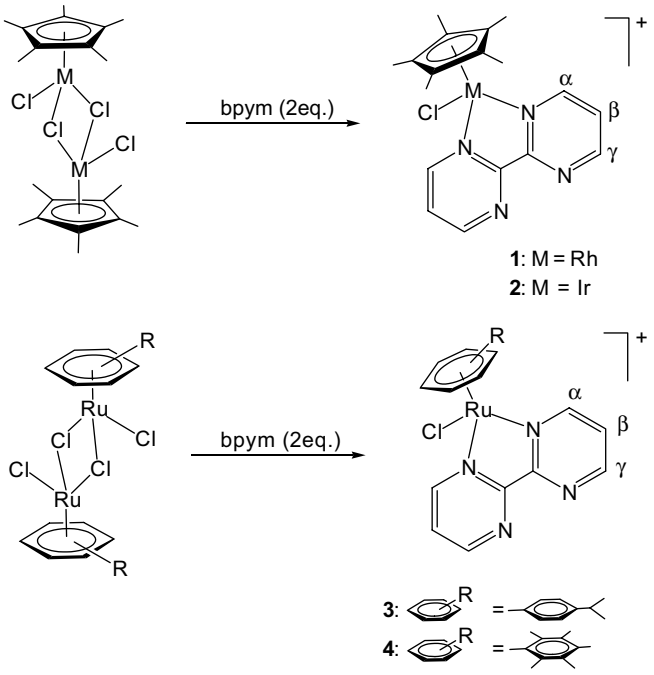

Scheme 1. Synthesis of cations **1**–**4**.

In the mass spectra they give, as expected, rise to the corresponding $[M]^+$ molecular peaks *m*/*z* at 431, 521, 429 and 457, respectively. The ^{1}H NMR spectra of complexes [**1**][PF$_6$], [**2**][PF$_6$] and [**4**][PF$_6$] exhibit a strong peak at $\delta = 1.75$, 1.73 and 2.15 ppm for the pentamethylcyclopentadienyl and hexamethylbenzene ligands, which are slightly shifted downfield in comparison to the starting complexes. The ^{1}H NMR spectrum of [**3**][PF$_6$] exhibits a doublet at $\delta = 1.13$ and a septet at $\delta = 2.81$ for the protons of the isopropyl group. The two doublets observed at $\delta = 6.37$–

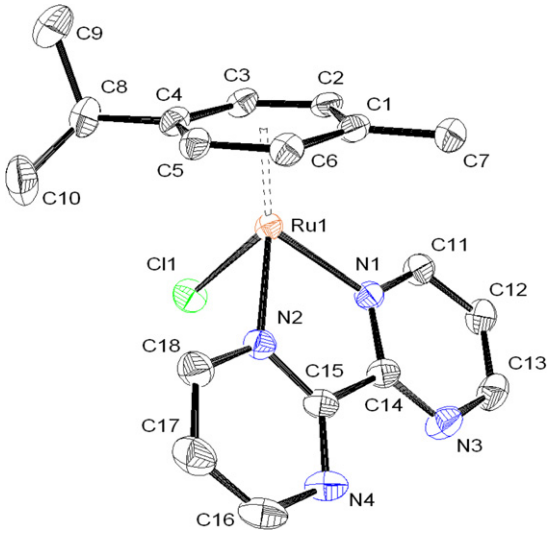

Fig. 1. Molecular structure of **3** at 50% probability level with hydrogen atoms and hexafluorophosphate anion omitted for clarity. Selected bond lengths (Å) and angles (°): Ru(1)–N(1) 2.084(2), Ru(1)–N(2) 2.080(3), Ru(1)–Cl(1) 2.3955(8), C(14)–C(15) 1.479(4); Cl(1)–Ru(1)–N(1) 85.43(6), Cl(1)–Ru(1)–N(2) 84.64(7), N(1)–Ru(1)–N(2) 77.12(9).

6.20 ppm correspond to the aromatic *p*-cymene ring CH protons. The α protons of the bpym ligand is shifted downfield in the cations **1**–**4** and appear as doublets of doublets (^3J coupling with H_β and ^4J coupling with H_γ) at $\delta \approx 9.30$ ppm for **1**, **2** and **4** and 10.30 ppm for **3**; in all cases the H_γ and H_β appears as doublets of doublets at around 9.1 and 7.9 ppm, respectively.

2.2. Crystal structure analysis of [(η⁶-p-Pr^{i}C$_6$H$_4$Me)RuCl(bpym)][PF$_6$] ([3][PF$_6$])

The molecular structure of [(η^6-*p*-Pr^{i}C$_6$H$_4$Me)RuCl(bpym)]$^+$ (**3**) has been established by single-crystal X-ray structure analysis of the [**3**][PF$_6$] salt. The complex shows a typical piano-stool geometry with the metal centre coordinated by the aromatic ligand, a terminal chloride and a chelating *N*,*N*-ligand (see Fig. 1). The Ru–N bond distances [2.084(2) and 2.080(3) Å] in **3** are comparable to those in [(η^6-*p*-Pr^{i}C$_6$H$_4$Me)RuCl(2,3-bis(2-pyridyl)pyrazine)][BF$_4$] [9] and [(η^6-*p*-Pr^{i}C$_6$H$_4$Me)RuCl(2,3-bis(α-pyridyl)quinoxaline)][PF$_6$] [10]. Accordingly, there is no significant difference in the Ru–Cl bond length in **3** [2.3955(8) Å] and reported values [9–11]. The N(1)–Ru(1)–N(2) bond angle in complex **3** [77.12(9)°] is similar to those of complexes [(η^6-*p*-Pr^{i}C$_6$H$_4$Me)RuCl(2,3-bis(2-pyridyl)pyrazine)]$^+$ [N(1)–Ru(1)–N(2) = 76.5(2)°] [9] and [(η^6-*p*-Pr^{i}C$_6$H$_4$Me)RuCl(2,3-bis(α-pyridyl)quinoxaline)]$^+$ [N(1)–Ru(1)–N(2) = 76.2(2)°] [10]. The angle between the least-square planes of η^6-C$_6$H$_4$ and that of bpym is 54.53(8)° and compares well with that of the analogous complex [(η^6-C$_6$Me$_6$)RuCl(2,2′-bipyridine)(OH$_2$)]$^{2+}$ which possesses an angle of 52.5(1)° between the η^6-C$_6$Me$_6$ and 2,2′-bipyridine planes [4].

In the crystal, two molecules of **3** form a dimer through C–H···Cl contacts, see Fig. 2. The closest C···Cl separations are 3.554(3), 3.730(3) and 3.737(3) Å with C–H···Cl angles of 127.1, 144.0 and 112.3°, respectively. The distance observed between the two Ru centres of the dimer is 5.810(1) Å and excludes metal–metal interactions.

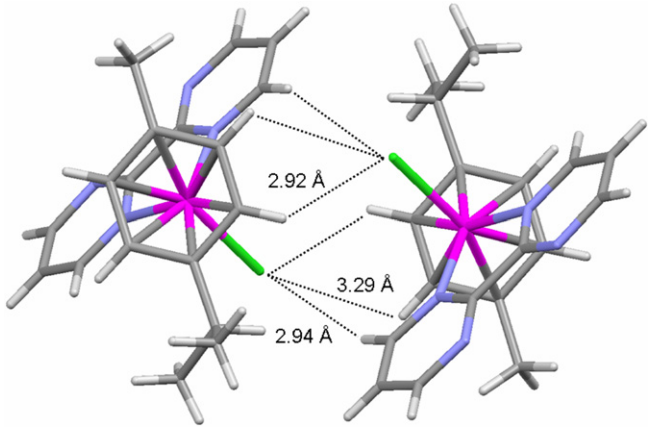

Fig. 2. Dimeric structure of **3** showing the intermolecular hydrogen contacts.

2.3. Synthesis of the dinuclear complexes 5–8

The reaction of the dimeric chloro complexes [(η^5-C$_5$Me$_5$)MCl$_2$]$_2$ (M = Rh, Ir) and [(η^6-arene)RuCl$_2$]$_2$ (arene = *p*-Pr^{i}C$_6$H$_4$Me, C$_6$Me$_6$) with 1 equiv. of 2,2′-bipyrimidine (bpym) in methanol results in the formation of the orange coloured, air-stable dinuclear complex dications [{(η^5-C$_5$Me$_5$)RhCl}$_2$(bpym)]$^{2+}$ (**5**), [{(η^5-C$_5$Me$_5$)IrCl}$_2$(bpym)]$^{2+}$ (**6**), [{(η^6-*p*-Pr^{i}C$_6$H$_4$Me)RuCl}$_2$(bpym)]$^{2+}$ (**7**) and [{(η^6-C$_6$Me$_6$)RuCl}$_2$(bpym)]$^{2+}$ (**8**), which can be isolated as their hexafluorophosphate or triflate salts (Scheme 2).

Complexes **5**–**8** were characterised by mass, ^{1}H NMR spectroscopy and elemental analysis. In the mass spectra the hexafluorophosphate salts give rise to two main peaks; a minor peak with an approximately 50% intensity attributed to [M^{2+} + PF$_6^-$]$^+$ at *m*/*z* 895, 1029, 845 and 900, respectively, and a major peak which corresponds after decomplexation of an [(arene)MCl]$^+$ fragment to the mononuclear cations **1**–**4** at *m*/*z* = 431, 521, 429 and 457, respectively.

The ^{1}H NMR spectra of [**5**][PF$_6$]$_2$ and [**8**][PF$_6$]$_2$ are complex due to the presence of *cis* and *trans* isomers (ratio ≈ 1:1), as far as the position of the chloro ligands with respect to each other are concerned. However, in the case of [**6**][PF$_6$]$_2$ and [**7**][PF$_6$]$_2$, the simplicity of the ^{1}H NMR spectrum indicates the presence of only one isomer. The osmium analogues show a similar behaviour, the dinuclear *p*-cymene derivative [{(η^6-*p*-Pr^{i}C$_6$H$_4$Me)OsCl}$_2$(bpym)]$^{2+}$ being formed exclusively as the *trans* isomer, while the hexamethylbenzene

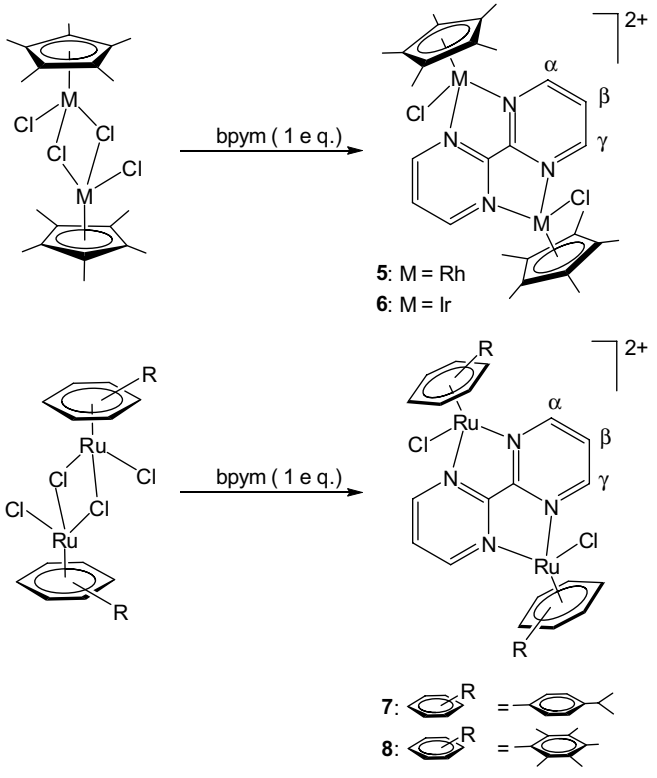

Scheme 2. Synthesis of the dications **5**–**8**.

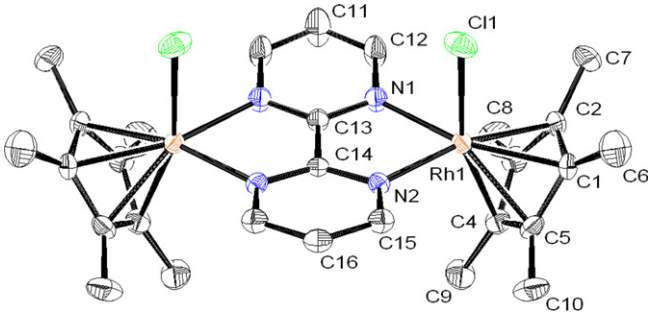

Fig. 3. Molecular structure of **5** at 50% probability level with hydrogen atoms and hexafluorophosphate anions omitted for clarity. Selected bond lengths (Å) and angles (°): Rh(1)–Rh(1)^{i} 5.745(1), Rh(1)–Cl(1) 2.405(2), Rh(1)–N(1) 2.134(5), Rh(1)–N(2) 2.161(5), C(13)–C(14) 1.47(1); N(1)–Rh(1)–N(2) 76.5(2), Cl(1)–Rh(1)–N(1) 85.29(15), Cl(1)–Rh(1)–N(2) 85.79(14). Symmetry operation: (i) $-x$, y, z.

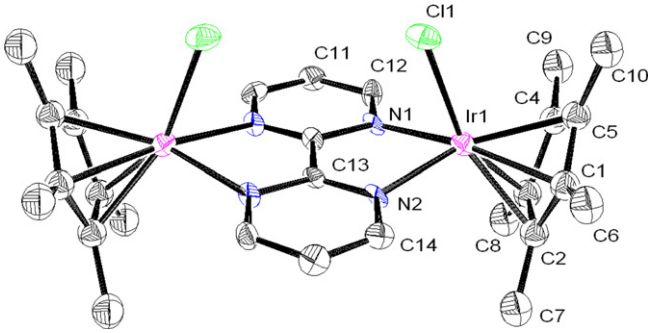

Fig. 4. Molecular structure of **6** at 50% probability level with hydrogen atoms and triflate anions omitted for clarity. Selected bond lengths (Å) and angles (°): Ir(1)–Ir(1)^{i} 5.636 (1), Ir(1)–Cl(1) 2.385(3), Ir(1)–N(1) 2.128(8), Ir(1)–N(2) 2.166(8), C(13)–C(13)^{i} 1.44(2); N(1)–Ir(1)–N(2) 77.1(3), Cl(1)–Ir(1)–N(1) 82.8(2), Cl(1)–Ir(1)–N(2) 82.9(2). Symmetry operation: (i) $0.5-x$, $1.5-y$, z.

derivative $[\{(\eta^6\text{-}C_6Me_6)OsCl\}_2(bpym)]^{2+}$ is formed as a mixture of *cis* and *trans* isomers [11]. As the single-crystal X-ray analysis of $[\mathbf{7}][PF_6]_2$ shows **7** to be present as the *trans* isomer in the solid state, we believe that the single isomer present in solution is also the *trans* isomer.

*2.4. Molecular structures of $[\{(\eta^5\text{-}C_5Me_5)RhCl\}_2(bpym)]^{2+}$ (**5**), $[\{(\eta^5\text{-}C_5Me_5)IrCl\}_2(bpym)]^{2+}$ (**6**) and $[\{(\eta^6\text{-}p\text{-}Pr^iC_6H_4Me)RuCl\}_2(bpym)]^{2+}$ (**7**)*

The compounds $[\mathbf{5}][PF_6]_2$ and $[\mathbf{6}][CF_3SO_3]_2$ crystallise in the orthorhombic space groups *Cmcm* and *Pccn*, while compound $[\mathbf{7}][PF_6]_2$ crystallises in the monoclinic space group $P2_1/n$. ORTEP drawings with the atom labelling scheme for the complexes **5**–**7** are shown in Figs. 3–5 together with selected bond lengths and angles. Complexes **5**–**7** contain two metal centres (Rh(III), Ir(III) or Ru(II)) bonded to an η^5-C_5Me_5 or η^6-*p*-$Pr^iC_6H_4Me$ ligands, respectively, which are bridged by the bpym ligand through its nitrogen atoms. Interestingly, the dinuclear cations **5** and **6** reveal a *cis* conformation of the two chloro ligands, while only the *trans* isomer is observed in the case of **7**.

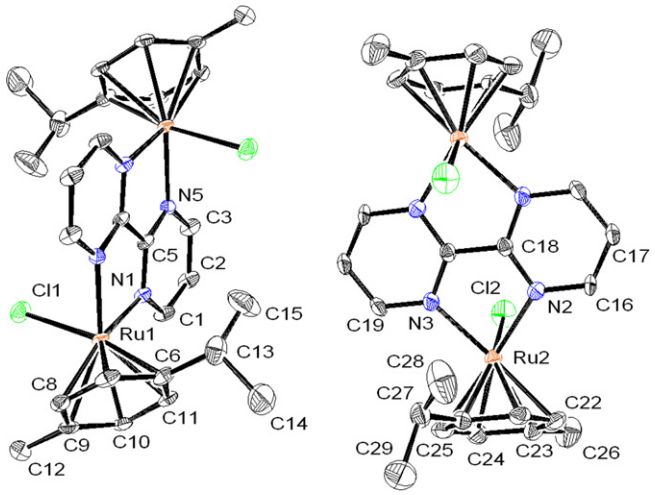

Fig. 5. Molecular structure of **7** showing the two independent molecules at 50% probability level with hydrogen atoms and hexafluorophosphate anions omitted for clarity. Selected bond lengths (Å) and angles (°): Ru(1)–Ru(1)^{i} 5.662(1), Ru(1)–N(1) 2.113(3), Ru(1)–N(5) 2.106(3), Ru(1)–Cl(1) 2.392(1), C(5)–C(5)^{i} 1.450(6), Ru(2)–Ru(2)^{ii} 5.687(2), Ru(2)–N(2) 2.117(3), Ru(2)–N(3) 2.122(3), Ru(2)–Cl(2) 2.384(1), C(18)–C(18)^{ii} 1.433(7); N(1)–Ru(1)–N(5) 78.07(10), N(1)–Ru(1)–Cl(1) 84.32(8), N(5)–Ru(1)–Cl(1) 83.51(8), N(2)–Ru(2)–N(3) 77.49(11), N(2)–Ru(2)–Cl(2) 82.69(8), N(3)–Ru(2)–Cl(2) 83.92(8). Symmetry operations: (i) $-x$, $-y$, $-z$, (ii) $1-x$, $-y$, $-z$.

The average distances between the metal atom and the carbon atoms of the η^5-C_5Me_5 ring are identical in **5** and **6** at 2.17 Å. These bond lengths are comparable to those in related η^5-C_5Me_5 rhodium and iridium complexes such as $[(\eta^5\text{-}C_5Me_5)IrCl((S)\text{-}1\text{-phenylethylsalicylaldiimine})]$ [2.17 Å] and $[(\eta^5\text{-}C_5Me_5)RhCl((S)\text{-}1\text{-phenylethylsalicylaldiimine})]$ [2.16 Å] [12]. The M–Cl bond lengths are 2.4048(13) Å (in **5**) and 2.4086(8) Å (in **6**), which are almost identical to the reported cationic poly-pyridyl rhodium complex $[(\eta^5\text{-}C_5Me_5)RhCl(4'\text{-phenyl-}2,2':6',2'\text{-terpyridine})]^{+}$ [2.3984(1) Å] [13].

The unit cell of compound $[\mathbf{7}][PF_6]_2$ contains two independent centrosymmetric molecules with *trans* configuration of the two chloro ligands, as shown in Fig. 5. The Ru–N bond distances ranging from 2.106(3) to 2.122(3) Å are longer than in the mononuclear complex **3** [2.084(2) and 2.080(3) Å], while the ruthenium-chlorine bond distances are comparable. In both cases, the isopropyl group of the *p*-cymene ligand is located opposite to the halide ligand in order to limit steric interaction. Therefore, the main difference between the two independent molecules resides in the relative position of the methyl group of the *p*-cymene with the terminal chloro ligand: In the first molecule the Cl(1)–Ru(1)–C(9)–C(12) torsion angle is 9.0(3)°, while in the other molecule the corresponding torsion angle is 19.9(4)° [Cl(2)–Ru(2)–C(23)–C(26)].

Upon formation of mono or dinuclear complexes, the bond lengths between the two connecting carbon atoms of the bpym ligand are reduced. Indeed, as compare to the free 2,2′-bipyrimidine in which the C–C distance is 1.501(1) Å [14,15], the C–C distance in the mononuclear

complex **3** is 1.479(4) Å while in the dinuclear complexes **5**, **6** and **7** the distances are 1.47(1), 1.44(2) and 1.433(7) Å, respectively. These bond length changes are in agreement with a back-donation from the metallic fragments to the bpym system, thus increasing the inter-ring bond order [11,15].

2.5. Stability of complexes *1–8* in solution

It is well known that coordinating solvents can replace terminal chloro ligands in arene ruthenium complexes [16]. In order to examine the stability of the chloro complexes **1–8** in solution, we recorded the ^{1}H NMR spectra in various deuterated solvents with different coordinating ability. At room temperature or even at elevated temperature, ^{1}H NMR experiments for **1–8** in dichloromethane-d_2, acetone-d_6, acetonitrile-d_3 and *N*,*N*-dimethylformamide-d_7 show no signal changes indicative of the replacement of the chloro ligands or the presence of free bpym units. Similarly in D_2O at room temperature no signal changes are observed for **1–8**, however after addition of formic acid and heating the aqueous solution at 50 °C for 1 h, a slight shift of the signals takes place suggesting the formation of formiato intermediates as proposed in the catalytic cycle [4].

Table 1
Summary of electrochemical data for the mononuclear complexes $[(arene)M(bpym)Cl]^+$ (**1–4**)[a]

Cation	E_{pc}(A) [$E_{1/2}$]/V	E_{pa}(B)/V	E_{pc}/V
1	−0.74 [−0.71]	−0.45	ca. −1.85
2	−0.82 [−0.79]	−0.37	ca. −2.00
3	−0.83 [−0.81]	−0.45	ca. −1.99
4	−0.90 [−]	−0.53	Not detected

[a] Peak potentials (E_{pa}, E_{pc}) from cyclic voltammograms recorded at 100 mV s^{-1} scan rate on a platinum disc electrode; half-wave potentials ($E_{1/2}$) from voltammetry at 20 mV s^{-1} on RDE. The potentials are given relative to saturated calomel electrode. See Section 3 for details. The assignment follows that given in the text and Fig. 6.

2.6. Electrochemistry of complexes *1–8*

The electrochemical behaviour of **1–8** was studied by cyclic voltammetry at platinum disc and by voltammetry at rotating platinum disc electrode (RDE) using ca. 5×10^{-4} M *N*,*N*-dimethylformamide (DMF) solutions containing 0.1 M tetrabutylammonium hexafluorophosphate as the supporting electrolyte. The pertinent data are summarised in Tables 1 and 2 for the mono and dinuclear complexes, respectively [17].

The redox responses of all mononuclear complexes (**1–4**) are similar (Fig. 6), not differing from those reported previously for $[(arene)MCl(bipy)]^+$ ((arene)M = (η^5-C_5Me_5)Rh, (η^5-C_5Me_5)Ir, and (η^6-arene)Ru; bipy = 2,2′-bipyridine) and $[(\eta^5\text{-}C_5Me_5)MCl(bpym)]^+$ (M = Rh, Ir) cations in acetonitrile solutions [18]. In all cases, the first reductions waves (A) represent two-electron irreversible processes (up to 500 mV s^{-1}) which are diffusion-controlled as evidenced by $i_p \propto v^{1/2}$ (in cyclic voltammetry) and $i_{lim} \propto \omega^{1/2}$ (in voltammetry at Pt-RDE). Their associated oxidative peaks (B) also show diffusion control ($i_p \propto v^{1/2}$) but with peak currents lower than those of the corresponding reduction wave.

Table 2
Summary of electrochemical data for the dinuclear complexes $[\{(arene)M\}_2(bpym)Cl_2]^{2+}$ (**5–8**)[a]

Cation	E_p/V [$E_{1/2}$/V] (wave)
5	E_{pc}: ca. −0.39 (A), −0.74 (B), −0.89 (C); E_{pa}: −0.43 (D), −0.11 (E)
6	E_{pc}: −0.29 (A), −0.75 (B), −1.09 (C); E_{pa}: −0.39 (D), −0.09 (E)
7	E_{pc}: −0.29 (A), −0.79 (B), −1.08 (C); E_{pa}: −0.22 (D) [$E_{1/2}$ −0.26], ca. −0.12 (E), −0.45 (F), −0.70 (G)
8[b]	E_{pc}: −0.36 (A), −0.90 (B), −1.16 (C); E_{pa}: −0.29 (D) [$E_{1/2}$ −0.32], ca. −0.17 (E), −0.53 (F)[c]

[a] Peak potentials (E_{pa}, E_{pc}) from cyclic voltammograms recorded at 100 mV s^{-1} scan rate on a platinum disc electrode. The potentials are given relative to saturated calomel electrode. See Section 3 for details. The assignment follows that given in the text and Fig. 6a and c.

[b] The G wave is hardly detectable for **8**.

[c] The reduction is observed with full reversibility when the switching potential is set before the following reduction peak; $E_{pa} = -0.21$ V.

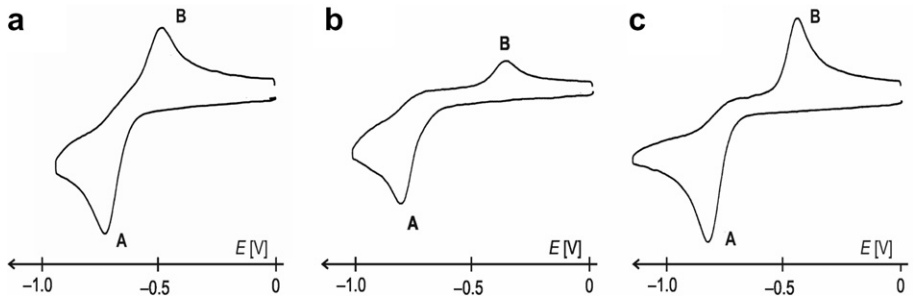

Fig. 6. Cyclic voltammograms of **1** (a), **2** (b), and **3** (c), recorded in *N*,*N*-dimethylformamide solutions on a platinum disc at 100 mV s^{-1}.

This behaviour can be explained by a fast reductive loss of the chloride ligand in an ECE process leading to neutral [(arene)M(bpym)] species (Eq. (1); (arene)M = (η^5-C_5H_5)Rh, (η^5-C_5H_5)Ir, and (η^6-arene)Ru), as it has been proposed for the [(arene)MCl(bipy)]$^+$ and [(arene)MCl(bpym)]$^+$ cations [18]:

$$[(\text{arene})\text{M}(\text{bpym})\text{Cl}]^+ + 2e^- \rightarrow [(\text{arene})\text{M}(\text{bpym})] + \text{Cl}^- \quad (1)$$

The reduced species undergo irreversible oxidation at still negative potentials (wave B in Fig. 6). However, since the redox response does not change upon addition of Cl^- ions in large excess (as solid [Bu_4N][Cl]) to the analysed solution, we attribute the B peak to the oxidation of [(arene)M(bpym)] to other yet unknown product(s) without recovery of the parent compound [19].

Quite expectedly, the redox potentials of the mononuclear cations vary with both, the metal and the supporting ligands. The rhodium(III) complex **1** is reduced more easily than its iridium(III) analogue **2**, whereas the reduction of the ruthenium complexes reflects the donating ability of the arene donors, as **3** featuring the less electron-donating *p*-cymene donor is reduced less negatively than its fully ring-alkylated counterpart **4**. Both observations parallel the trends observed in the series of analogous 2,2′-bipyridine complexes (vide supra) [18].

The mononuclear compounds exert additional, partly reversible reductions at very negative potentials (located at 1.11–1.18 V more negatively vs. A; wave not detectable for **4**). These processes are attributable to reduction of the electro-chemically generated neutral species [(arene)M(bpym)], localised most likely at the bpym ligand.

In summary, the reduction behaviour of the mononuclear complexes is mechanistically similar. The voltammograms differ mainly by the position of the waves (vide supra), reduction–oxidation 'hysteresis' (i.e., in $E_{pc}(A) - E_{pa}(B)$ difference) and relative heights of the associated peaks (i.e., by $i_{pc}(A)/i_{pa}(B)$ ratio), which probably relate to a different stability of the electrogenerated, low-valent products.

When compared with their mononuclear counterparts, the dinuclear complexes exhibit a more complex electrochemical behaviour. This is not only due to the presence of two metal centres but also because of configurational isomerism and possible splitting of the dimeric structure into two redox active mononuclear cations [(arene)MCl(bpym)]$^+$ and [(arene)MCl(solvent)$_x$]$^+$. It has been shown that in acetonitrile the dications [(η^5-C_5Me_5)$_2$$M_2$-$Cl_2$(bpym)]$^{2+}$ (M = Rh, Ir) are first reduced (1e) to the corresponding monocations [(η^5-C_5Me_5)$_2$$M_2Cl_2$(bpym)]$^+$, whose subsequent single-electron reduction triggers the loss of halide, thus yielding [(η^5-C_5Me_5)$_2$$M_2$Cl(bpym)]$^+$. The latter species loose the remaining halide anion in a subsequent two-electron reduction to give neutral species [(η^5-C_5Me_5)$_2$$M_2$(bpym)]. This chloride-free compound is reduced at even more negative potentials [20]. On the other hand, the reduction pattern observed for diosmium [{(η^6-*p*-$Pr^iC_6H_4Me$)OsCl}$_2$(bpym)][PF_6]$_2$ was interpreted as consisting of two consecutive one-electron reductions followed by electrochemically irreversible reduction accompanied by the loss of the halide ion [11].

The change of the solvent for *N*,*N*-dimethylformamide may influence dissociative equilibria and, hence, the overall redox response [21]. The first reduction of the dirhodium(III) complex **5** is observed as a broad wave at around −0.39 (A) V, followed by two reductive waves at −0.74 (B) and −0.89 (C) V (Fig. 7a and b). Upon scanning to more negative potentials, two additional, reversible reductions are observed at −1.82 and −1.96 V. The nature of the most negative reductions is difficult to judge, as they occur at the onset of the base electrolyte decomposition and, hence, will not be discussed in detail [22].

The first reduction process (A) is irreversible, giving rise to an oxidative peak at −0.11 V (E). The following reduction at −0.74 V (B) is irreversible as well, involving chemical steps that relatively slowly generate an oxidisable though rather unstable product reflected by an anodic wave at −0.43 V (D). Anodic wave D is not detectable during an immediate back scan at 100 mV s^{-1} when the switching potential set just after the B wave (−0.80 V), but emerges in scans performed at the same scan rate after a short electrolysis at the switching potential or when the scan extends further beyond the C wave (Fig. 7b). The instability of the electro-chemically generated product is manifested by an

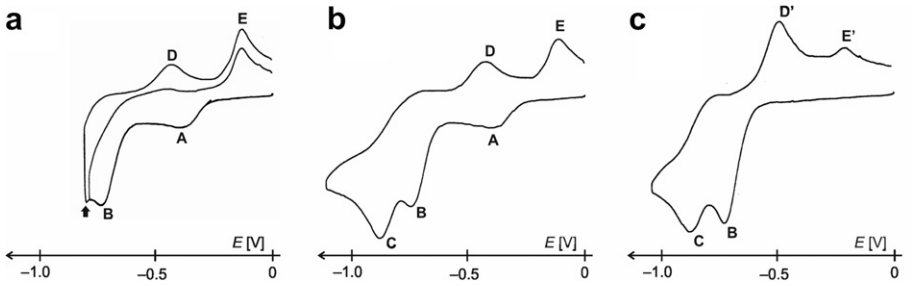

Fig. 7. Cyclic voltammograms of **5** recorded in an *N*,*N*-dimethylformamide solution on a platinum disc at 100 mV s^{-1} over different potential ranges (a, b). Note the differences observed after electrolysis (a; electrolysis performed at the potential indicated with an arrow for 10 s), and after addition of [Bu_4N][Cl] (c).

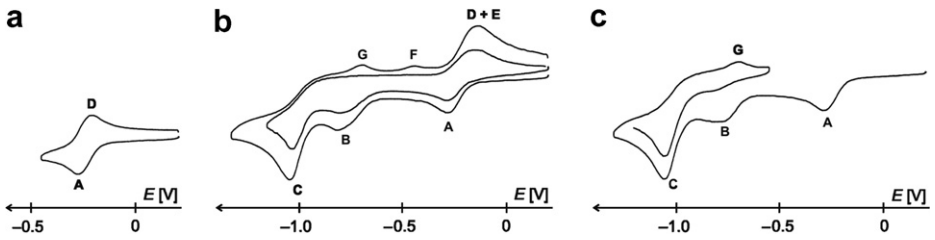

Fig. 8. Cyclic voltammograms of **7** recorded in an *N*,*N*-dimethylformamide solution on a platinum disc at 100 (a and c; for b *outer* trace only) and 50 mV s^{-1} (b *inner* trace).

absence of the D wave in cyclic voltammograms recorded at relatively slower scan rates (e.g., at 20 mV s^{-1}). Furthermore, similarity of the potentials for the B–D waves with those of **1** suggests involvement of the mononuclear complex (vide supra).

It is noteworthy that an addition of $[Bu_4N][Cl]$ in a large molar excess to the analysed solutions leads to a disappearance of the first reduction wave (A) and a shift of the anodic waves (E′: −0.21 V, D′: −0.50 V), whereas the B and C reduction waves are observed practically intact (Fig. 7c). This, together with a concurrent increase of the peak current due to B (i.e., $i_p(A) + i_p(B)$ without added chlorides $\approx i_p(B)$ with added chlorides), allows to attribute wave A to a reduction of a decomposition product. The redox behaviour of the iridium congener **6** is similar but with the waves shifted towards more negative potentials and influenced by adsorption phenomena.

The diruthenium complex **7** displays a reversible, one-electron wave at −0.26 V (A/D). Upon increasing the switching potential in cyclic voltammetry, there are observed another one-electron wave at −0.79 V (B) and an irreversible, two-electron reduction at −1.08 V (C) (Fig. 8). During the back scan, new minor anodic peaks at −0.45 V (F) and −0.70 V (G) emerge and the oxidation wave corresponding to the first reduction (i.e., wave D) appears *convoluted* with another oxidative wave at ca. −0.12 V (E). While wave G occurs only when the scan is performed with switching potential set after the second reductive wave (C) (Fig. 8b), the anodic peak F is only observable at relatively faster scan rates (e.g., not at 50 mV s^{-1}) and during fast back scan (e.g., during reduction at 100 mV s^{-1} and reoxidation at 500 mV s^{-1}). In addition, peak F is observed neither after electrolysis at a potential set just after the B reduction wave (−0.30 V for 10 s) nor during repeated cycling over B wave even at low scan rates, which makes it clearly attributable to a product arising from the third reduction (C) and coupled chemical reactions. As in the previous case, the similarity of the potentials due to peaks B and F with the potentials observed for the mononuclear analogue suggest the latter to be a part of the overall redox response.

The redox behaviour of **8** is roughly similar to that of **7** but with the peaks observed in different relative proportion and, in accordance with an increased donor ability of the arene ring, shifted to more negative potentials (cf. the mononuclear ruthenium complexes above).

Table 3
Catalytic transfer hydrogenation of acetophenone using the mononuclear $[(arene)M(bpym)Cl]^+$ (**1**–**4**) and dinuclear complexes $[\{(arene)M\}_2(bpym)Cl_2]^{2+}$ (**5**–**8**) as catalysts and formate as hydrogen donor in water [a]

Entry	Catalyst	(arene)M	conversion % (h)[b]	TOF (h^{-1})[c]
1	**1**	$(C_5Me_5)Rh$	99 (15)	10.5
2	**2**	$(C_5Me_5)Ir$	76 (14)	5
3	**3**	$(p\text{-}MeC_6H_4{}^iPr)Ru$	21 (14)	2
4	**4**	$(C_6Me_6)Ru$	7 (14)	0.5
5	**5**	$\{(C_5Me_5)Rh\}_2$	98 (8)	19
6	**6**	$\{(C_5Me_5)Ir\}_2$	99 (10)	14
7	**7**	$\{(p\text{-}MeC_6H_4{}^iPr)Ru\}_2$	82 (14)	10.5
8	**8**	$\{(C_6Me_6)Ru\}_2$	20 (14)	2

[a] Conditions: Reactions carried out at 50 °C, at pH 4, in 5 mL of water, acetophenone (0.64 mmol), the ratio catalyst/substrate/formate being 1/100/500.
[b] Determined by gas chromatography.
[c] TOF: turnover frequencies taken at 30% of conversion and expressed in mol of product/(mol of Ru · h).

2.7. Catalytic application of *1*–*8* for the transfer hydrogenation of acetophenone in aqueous solution

Based on the pioneering study of Ogo et al. on the use of bipyridine (bipy) complexes $[(C_6Me_6)Ru(bipy)(OH_2)]^{2+}$ [4] and $[(C_5Me_5)Ir(bipy)(OH_2)]^{2+}$ [23] and on our previously reported results on arene ruthenium phenanthroline (phen) complexes $[(arene)Ru(phen)(OH_2)]^{2+}$ (arene = C_6H_6, *p*-$Pr^iC_6H_4Me$, C_6Me_6) [6,24], the catalytic potential of the 2,2′-bipyrimidine complexes **1**–**8** was evaluated for the transfer hydrogenation of acetophenone in water using formic acid as hydrogen source. It is worth mentioning that the triflate salt of **2** ($[\mathbf{2}][CF_3SO_3]$) has been recently used for the catalytic aerobic oxidation of alcohols to aldehydes involving, however, a different catalytic mechanism [25].

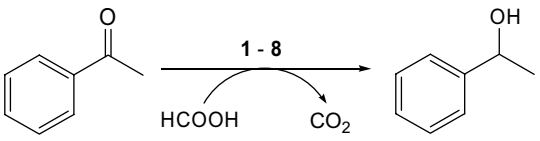

All complexes were found to catalyse the transfer hydrogenation of acetophenone to give phenylethanol in aqueous solution (Table 3). As expected, the dinuclear complexes show higher activity than the corresponding mononuclear complexes. The best results were found with rhodium for

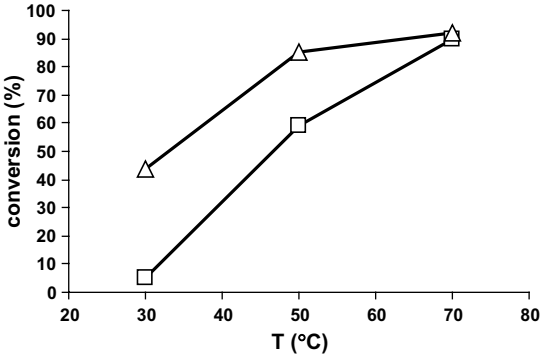

Fig. 9. Temperature-dependent profile of conversion using **1** (□) or **5** (△) as catalyst and formate as hydrogen donor in water (5 mL) for transfer hydrogenation of acetophenone (0.64 mmol), at pH 4, for 4 h, the catalyst/substrate/formate ratio being 1/100/500.

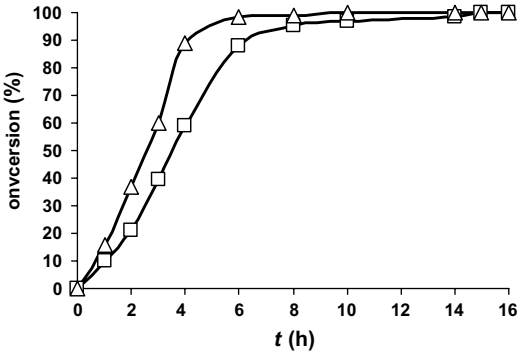

Fig. 11. Time dependence of conversion using **1** (□) or **5** (ρ) as catalyst and formate as hydrogen donor in water (5 mL) for transfer hydrogenation of acetophenone (0.64 mmol), at 50 °C, at pH 4, the catalyst/substrate/formate ratio being 1/100/500.

the both mono and dinuclear complexes series with turnover frequencies of 10.5 h^{-1} for **1** and 19 h^{-1} for **5** at 50 °C: The dinuclear complex **5** (*cis* and *trans* isomers in solution) shows an activity almost two times higher than that found with the corresponding mononuclear complex **1** (entries 1 and 5), which corresponds in a first approximation to additive contribution of the two rhodium centres to the catalytic activity. The modest activities of the hexamethylbenzene ruthenium complexes **4** and **8** (*cis* and *trans* isomers in solution), are astonishing in light of the activities found for the corresponding bipyridine [4] and phenanthroline [6] complexes.

Surprisingly, the dinuclear iridium complex **6** (*trans* isomer) shows a catalytic activity almost three times higher than that found with the corresponding mononuclear complex **2** (entries 2 and 6). Similarly, the dinuclear *p*-cymene ruthenium complex **7** (*trans* isomer) shows an almost five times higher catalytic activity as compared to the corresponding mononuclear complex **3** (entries 3 and 7). The temperature-dependence study, using the rhodium complexes **1** and **5** (Fig. 9) reveal that the difference between catalytic activities of mono and dinuclear complexes increase at temperatures lower than 50 °C. At 30 °C, the dinuclear rhodium complex **5** shows a more than four times

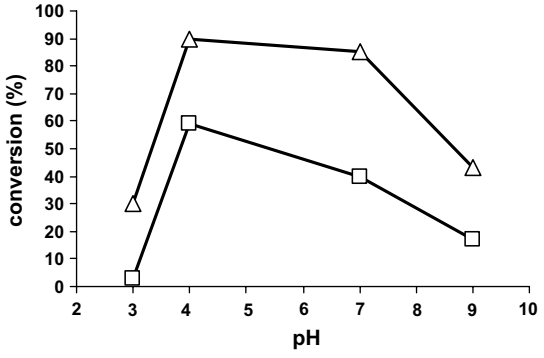

Fig. 10. pH-Dependent profile of conversion using **1** (□) or **5** (△) as catalyst and formate as hydrogen donor in water (5 mL) for transfer hydrogenation of acetophenone (0.64 mmol), at 50°C, for 4 h, the catalyst/substrate/formate ratio being 1/100/500.

higher catalytic activity than that observed with mononuclear complex **1**. This may be explained by a synergistic electronic effect of the second metal centre on the first one through the π-system of the bridging ligand, particularly pronounced in the *trans* isomer.

The pH dependence of the catalytic activity was also studied in the case of **1** and **5** for same reaction. As Fig. 10 shows, the best pH conditions were found in the both two cases to be around 4, which correspond to the pK_a of the formic acid (3.77). At this pH, formic acid and formate are in 1:1 equilibrium.

The kinetic plot (Fig. 11) shows that, at 50 °C and for pH 4, the reaction is almost complete after 8 h for **1** and after 6 h for **5**. The initial turnover frequency calculated in this case for the best catalyst precursor **5** is 19 h^{-1}; lower than those previously found with the bipyridine (75 h^{-1}) [4] or the phenanthroline mononuclear complexes (32 h^{-1}) [6].

In conclusion, the catalytic hydrogenation activity of the mononuclear complexes is in line with the electrochemical measurements: the TOF values decrease with decreasing of the first reduction potential (wave A). In other words, the easiest reducible complexes show the highest catalytic activities, which is reasonable, given that the mechanism suggested involves hydride intermediates. The dinuclear complexes show the same cyclovoltammetric trends as their mononuclear congeners (wave B), their electrochemical behaviour, however, being complicated by other phenomena. The increase of the catalytic activity by three to five times in going from the mononuclear complexes to their dinuclear congeners may be accounted for by a synergistic electronic effect in the intact dinuclear complexes.

3. Experimental

3.1. General

All reagents were purchased either from Aldrich or Fluka and used as received. $[M(\eta^5\text{-}C_5Me_5)(\mu\text{-}Cl)Cl]_2$ (M = Rh, Ir) [26], $[Ru(\eta^6\text{-}p\text{-}Pr^iC_6H_4Me)(\mu\text{-}Cl)Cl]_2$ [27], $[Ru(\eta^6\text{-}C_6Me_6)(\mu\text{-}Cl)Cl]_2$ [28] were prepared according to

published methods. The NMR spectra were recorded on a Varian Gemini 200 MHz or Bruker AMX 400 spectrometer using the residual protonated solvent as internal standard. Infrared spectra were recorded as KBr pellets on a Perkin–Elmer FTIR 1720-X spectrometer. Microanalyses were performed by the Laboratory of Pharmaceutical Chemistry, University of Geneva (Switzerland). Electrospray mass spectra were obtained in positive-ion mode with an LCQ Finnigan mass spectrometer.

3.2. Preparation of the mononuclear complexes *1*–*4*

3.2.1. *[(η^5-C_5Me_5)RhCl(bpym)][PF_6] ([**1**][PF_6])*

A mixture of [(η^5-C_5Me_5)Rh(μ-Cl)Cl]$_2$ (155 mg, 0.25 mmol), 2,2′-bipyrimidine (87 mg, 0.55 mmol) and potassium hexafluorophosphate (46 mg, 0.25 mmol) is suspended in methanol (20 mL) and stirred at room temperature. The solution becomes first clear, before the product precipitates. After 3 h the yellow solid is filtered, washed three times with diethylether (3 × 10 mL) and then dried in vacuo. Yield 150 mg, (52%). ^{1}H NMR (400 MHz, CD_3CN): δ (ppm) = 9.29 (dd, 2H, ^3J = 4.76 Hz, ^4J = 2.08 Hz, H_α), 9.17 (dd, 2H, ^3J = 5.64 Hz, H_γ), 7.96 (dd, 2H, H_β), 1.75 (s, 15H, C_5Me_5); IR (cm^{-1}): 1636(m), 1579(m), 1406(s), 1026(s), 847(s), 750(s), 558(s); ESI-MS: 431.1 [M^+], 395.1 [M − Cl]. Anal. Calc. for $C_{18}H_{21}ClN_4PF_6Rh$ (576.7): C, 37.49; H, 3.67; N 9.71. Found: C, 37.33; H, 3.57; N, 9.77%.

3.2.2. *[(η^5-C_5Me_5)IrCl(bpym)][PF_6] ([**2**][PF_6])*

The compound is prepared by the same procedure as described above for [**1**][PF_6] using [(η^5-C_5Me_5)Ir(μ-Cl)Cl]$_2$ (199 mg, 0.25 mmol), 2,2′-bipyrimidine (87 mg, 0.55 mmol) and potassium hexafluorophosphate (46 mg, 0.25 mmol). Orange–yellow solid, yield 175 mg, (53%). ^{1}H NMR (400 MHz, CD_3CN): δ (ppm) = 9.30 (dd, 2H, ^3J = 4.80 Hz, ^4J = 2.04 Hz, H_α), 9.14 (dd, 2H, ^3J = 5.72 Hz, H_γ), 7.95 (dd, 2H, H_β), 1.73 (s, 15H, C_5Me_5); IR (cm^{-1}): 1637(m), 1576(s), 1405(s), 1019(s), 847(s), 753(s), 558(s); ESI-MS: 521.1 [M^+]. Anal. Calc. for $C_{18}H_{21}ClN_4PF_6Ir$ (666.0): C, 32.46; H, 3.18; N, 8.41. Found: C, 32.53; H, 3.42; N, 8.60%.

3.2.3. *[(η^6-$C_{10}H_{14}$)RuCl(bpym)][PF_6] ([**3**][PF_6])*

A mixture of [(η^6-*p*-Pr^iC_6H_4Me)Ru(μ-Cl)Cl]$_2$ (153 mg, 0.25 mmol), 2,2′-bipyrimidine (87 mg, 0.55 mmol) and potassium hexafluorophosphate (46 mg, 0.25 mmol) is stirred in methanol (20 mL) at room temperature for 3 h, then filtered. The solvent is removed under vacuo. Then the residue is taken up in dichloromethane (5 mL) and filtered. The filtrate is concentrated (2 mL) and diethylether is slowly added to precipitate an orange–brown solid. Yield 170 mg, (59%). ^{1}H NMR (400 MHz, $CDCl_3$): δ (ppm) = 10.20 (dd, 2H, ^3J = 5.76 Hz, ^4J = 1.96 Hz, H_α), 9.18 (dd, 2H, ^3J = 4.76 Hz, H_γ), 7.93 (dd, 2H, H_β), 6.37 (d, 2H, ^3J = 6.44 Hz, $Ar_{p\text{-cym}}$), 6.20 (d, 2H, $Ar_{p\text{-cym}}$), 2.81 (sep, 1H, ^3J = 6.92 Hz, C**H**(CH_3)$_2$), 2.32 (s, 3H, CH_3), 1.13 (d, 6H, CH(C**H**$_3$)$_2$); IR (cm^{-1}): 1632(s), 1578(s), 1409(s), 845(s), 750(s), 558(s); ESI-MS: 429.0 [M^+]. Anal. Calc. for $C_{18}H_{20}ClN_4PF_6Ru$ (573.9): C, 37.67; H, 3.51; N, 9.76. Found: C, 37.24; H, 3.35; N, 9.42%.

3.2.4. *[(η^6-C_6Me_6)RuCl(bpym)][PF_6] ([**4**][PF_6])*

The compound is prepared by the same procedure as described above for [**1**][PF_6] using [(η^6-C_6Me_6)Ru(μ-Cl)Cl]$_2$ (167 mg, 0.25 mmol), 2,2′-bipyrimidine (87 mg, 0.55 mmol) and potassium hexafluorophosphate (46 mg, 0.25 mmol). Orange solid, yield 145 mg, (48%). ^{1}H NMR (400 MHz, CD_3CN): δ (ppm) = 9.20 (dd, 2H, ^3J = 4.72 Hz, ^4J = 2.00 Hz, H_α), 9.13 (dd, 2H, ^3J = 5.80 Hz, H_γ), 7.88 (dd, 2H, H_β), 2.15 (s, 18H, C_6Me_6); IR (cm^{-1}): 1632(m), 1577(s), 1406(s), 1022(m), 845(s), 749(s), 559(s); ESI-MS: 457.1 [M^+]. Anal. Calc. for $C_{20}H_{24}ClN_4PF_6Ru$ (601.9): C, 39.90; H, 4.01; N, 9.31. Found: C, 39.46; H, 4.24; N, 9.64%.

3.3. Preparation of the dinuclear complexes *5*–*8*

3.3.1. *[{(η^5-C_5Me_5)RhCl}$_2$(bpym)][PF_6]$_2$ ([**5**][PF_6]$_2$)*

A mixture of [(η^5-C_5Me_5)Rh(μ-Cl)Cl]$_2$(124 mg, 0.2 mmol), 2,2′-bipyrimidine (31.6 mg, 0.2 mmol) and potassium hexafluorophosphate (77 mg, 0.42 mmol) is suspended in methanol (20 mL) and stirred at room temperature. The solution becomes first clear, before the product precipitates. After 3 h the orange solid is filtered, washed three times with diethylether (3 × 10 mL) and then dried in vacuo. Yield 110 mg, (55%). The complex is formed as mixture of *cis* and *trans* isomers (ratio 1:1, ♦ and •) with respect to Cl atoms. ^{1}H NMR (200 MHz, Acetone-d_6): δ (ppm) = 9.86 (d, 4H, ^3J = 5.80 Hz, H_α) (♦), 9.72 (d, 4H, ^3J = 5.40 Hz, H_α) (•), 8.63 (dd, 2H, H_β) (♦), 8.48 (dd, 2H, H_β) (•), 1.92 (s, 30H, C_5Me_5) (♦), 1.88 (s, 30H, C_5Me_5) (•); IR (cm^{-1}): 1635(m), 1581(s), 1415(s), 843(s), 559(s); ESI-MS: 849.0 [$M^{2+} + PF_6^-$]$^+$. Anal. Calc. for $C_{28}H_{36}Cl_2N_4P_2F_{12}Rh_2$ (995.3): C, 33.79; H, 3.64; N, 5.62. Found: C, 33.53; H, 3.81; N, 5.66%.

3.3.2. *[{(η^5-C_5Me_5)IrCl}$_2$(bpym)][PF_6]$_2$ ([**6**][PF_6]$_2$)*

The compound is prepared by the same procedure as described above for [**5**][PF_6]$_2$ using [(η^5-C_5Me_5)Ir(μ-Cl)Cl]$_2$ (159 mg, 0.2 mmol), 2,2′-bipyrimidine (31.6 mg, 0.2 mmol) and potassium hexafluorophosphate (77 mg, 0.42 mmol). Orange solid, yield 155 mg, (66%). ^{1}H NMR (200 MHz, Acetone-d_6): δ (ppm) = 9.74 (d, 4H, ^3J = 5.50 Hz, H_α), 8.49 (dd, 2H, H_β), 1.90 (s, 30H, C_5Me_5); IR (cm^{-1}): 1632(s),1579(s), 1406(s), 844(s), 560(s); ESI-MS: 1028.9 [$M^{2+} + PF_6^-$]$^+$. Anal. Calc. for $C_{28}H_{36}Cl_2N_4P_2F_{12}Ir_2$ (1173.9): Anal. Calc. for C, 28.65; H, 3.09; N, 4.77. Found: C, 28.54; H, 3.26; N, 4.60%.

3.3.3. *[{(η^5-C_5Me_5)IrCl}$_2$(bpym)][CF_3SO_3]$_2$ ([**6**][CF_3SO_3]$_2$)*

A mixture of [(η^5-C_5Me_5)Ir(μ-Cl)Cl]$_2$ (159 mg, 0.2 mmol), 2,2′-bipyrimidine (31.6 mg, 0.2 mmol) and Ag(CF_3SO_3) (108 mg, 0.42 mmol) is stirred in methanol (20 mL) at room temperature. The solution becomes first

clear, before the product precipitates. After 3 h the orange solid precipitated and the product is filtered, washed three times with diethylether (3×10 mL) and then dried in vacuo. Orange solid, yield 140 mg (59%). ^{1}H NMR (200 MHz, Acetone-d_6): δ (ppm) = 9.72 (d, 4H, $^3J = 5.60$ Hz, H_α), 8.53 (dd, 2H, H_β), 1.89 (s, 30H, C_5Me_5); IR (cm^{-1}): 1632(m), 1413(s), 1264(s), 1030(s), 638(s); ESI-MS: 1033.1 $[M^{2+} + CF_3SO_3^-]^+$. Anal. Calc. for $C_{30}H_{36}Cl_2N_4S_2F_6O_6Ir_2$ (1182.1): C, 30.48; H, 3.07; N, 4.73. Found: C, 30.87; H, 3.01; N, 4.64%.

3.3.4. [{(η^6-$C_{10}H_{14}$)RuCl}$_2$(bpym)][PF_6]$_2$ ([7][PF_6]$_2$)

The compound is prepared by the same procedure as described above for [**5**][PF_6]$_2$ using [(η^6-*p*-Pr^{i}C$_6$H$_4$-Me)Ru(μ-Cl)Cl]$_2$ (122 mg, 0.2 mmol), 2,2′-bipyrimidine (31.6 mg, 0.2 mmol) and potassium hexafluorophosphate (77 mg, 0.42 mmol). Orange–yellow solid, yield 120 mg, (61%). ^{1}H NMR (200 MHz, Acetone-d_6): δ (ppm) = 10.15 (d, 4H, $^3J = 5.50$ Hz, H_α), 8.40 (dd, 2H, H_β), 6.48 (d, 4H, $^3J = 6.22$ Hz, $Ar_{p\text{-cym}}$), 6.24 (d, 4H, $Ar_{p\text{-cym}}$), 2.89 (sep, 2H, $^3J = 6.96$ Hz, $CH(CH_3)_2$), 2.33 (s, 6H, CH_3), 1.12 (d, 12H, $CH(CH_3)_2$); IR (cm^{-1}): 1638(s), 1582(s), 1418(s), 847(s), 558(s); ESI-MS: 845.0 $[M^{2+} + PF_6^-]^+$. Anal. Calc. for $C_{28}H_{34}Cl_2N_4P_2F_{12}Ru_2$ (989.6): C, 33.98; H, 3.46; N, 5.66. Found: C, 33.87; H, 3.17; N, 5.61%.

3.3.5. [{(η^6-C_6Me_6)RuCl}$_2$(bpym)][PF_6]$_2$ ([**8**][PF_6]$_2$)

The compound is prepared by the same procedure as described above for [**5**][PF_6]$_2$ using [(η^6-C_6Me_6)Ru(μ-Cl)Cl]$_2$ (134 mg, 0.2 mmol), 2,2′-bipyrimidine (31.6 mg, 0.2 mmol) and potassium hexafluorophosphate (77 mg, 0.42 mmol). Orange–yellow solid, yield 115 mg, (55%). The complex is formed as mixture of *cis* and *trans* isomers (ratio 1:1, ♦ and •) with respect to Cl atoms. ^{1}H NMR (200 MHz, Acetone-d_6): δ (ppm) = 9.71 (d, 4H, $^3J = 5.60$ Hz, H_α) (♦), 9.62 (d, 4H, $^3J = 5.80$ Hz, H_α) (•), 8.42 (dd, 2H, H_β) (♦), 8.39 (dd, 2H, H_β) (•), 2.31 (s, 36H, C_6Me_6) (♦), 2.26 (s, 36H, C_6Me_6) (•); IR (cm^{-1}): 1638(s), 1577(s), 1409(s), 846(s), 560(s); ESI-MS: 900.1 $[M^{2+} + PF^{6-}]^+$. Anal. Calc. for $C_{32}H_{42}Cl_2N_4P_2F_{12}Ru_2$ (1045.7): C, 36.75; H, 4.05; N, 5.35. Found: C, 36.34; H, 4.08; N, 5.30%.

3.4. Single-crystal X-ray structure analyses

Crystals of complexes [**3**][PF_6], [**5**][PF_6]$_2 \cdot (CH_3CN)_3$, [**6**][CF_3SO_3]$_2$ and [**7**][PF_6]$_2$ were mounted on a Stoe Image Plate Diffraction system equipped with a ϕ circle goniometer, using Mo Kα graphite monochromated radiation ($\lambda = 0.71073$ Å) with ϕ range 0–200°. The structures were solved by direct methods using the program SHELXS-97 [29]. Refinement and all further calculations were carried out using SHELXL-97 [30]. The H-atoms were included in calculated positions and treated as riding atoms using the SHELXL default parameters. Examination of the structures with platon [31] reveals in [**5**][PF_6]$_2 \cdot (CH_3CN)_3$ and [**6**][CF_3SO_3]$_2$ disordered solvent or anion molecules. Indeed, in [**5**][PF_6]$_2 \cdot (CH_3CN)_3$, three molecules of acetonitrile were found, but badly defined. Similarly in [**6**][CF_3SO_3]$_2$ a void corresponding to disordered triflate molecule was found. Therefore, new data sets corresponding to omission of the solvent or anions were generated

Table 4
Crystallographic and structure refinement parameters for complexes [**3**][PF_6], [**5**][PF_6]$_2 \cdot (CH_3CN)_3$, [**6**][O_3SCF_3]$_2$ and [**7**][PF_6]$_2$

	[**3**][PF_6]	[**5**][PF_6]$_2 \cdot (CH_3CN)_3$	[**6**][O_3SCF_3]$_2$	[**7**][PF_6]$_2$
Chemical formula	$C_{18}H_{20}ClF_6N_4PRu$	$C_{34}H_{45}Cl_2F_{12}N_7P_2Rh_2$	$C_{30}H_{36}Cl_2F_6N_4O_6S_2Ir_2$	$C_{28}H_{34}Cl_2F_{12}N_4P_2Ru_2$
Formula weight	573.87	1118.43	1182.05	989.57
Crystal system	Triclinic	Orthorhombic	Orthorhombic	Monoclinic
Space group	$P\bar{1}$ (no. 2)	*C mcm* (no. 63)	*Pccn* (no. 56)	$P2_1/n$ (no. 14)
Crystal colour and shape	Orange block	Orange rod	Red rod	Orange block
Crystal size	$0.36 \times 0.28 \times 0.17$	$0.21 \times 0.18 \times 0.08$	$0.32 \times 0.14 \times 0.12$	$0.27 \times 0.19 \times 0.16$
a (Å)	8.0068(9)	15.4901(10)	17.618(4)	16.912(3)
b (Å)	11.3491(13)	16.9110(13)	18.343(4)	13.181(3)
c (Å)	11.9571(13)	32.9008(19)	11.576(2)	18.232(4)
α (°)	83.789(13)			
β (°)	81.908(13)			117.62(3)
γ (°)	88.582(13)			
V (Å^3)	1069.4(2)	8618.5(10)	3741.0(13)	3601.1(13)
Z	2	8	4	4
T (K)	173(2)	173(2)	173(2)	173(2)
D_{calc} (g cm^{-3})	1.782	1.724	2.099	1.825
μ (mm^{-1})	0.998	1.052	7.439	1.166
Scan range (°)	$2.63 < \theta < 25.94$	$2.17 < \theta < 25.98$	$2.22 < \theta < 25.93$	$1.99 < \theta < 25.94$
Unique reflections	3887	4391	3352	6842
Reflections used [$I > 2\sigma(I)$]	3409	3282	2387	5820
R_{int}	0.0397	0.0806	0.0602	0.0340
Final R indices [$I > 2\sigma(I)$][a]	0.0304, wR_2 0.0749	0.0608, wR_2 0.1364	0.0365, wR_2 0.0977	0.0288, wR_2 0.0664
R indices (all data)	0.0354, wR_2 0.0768	0.0779, wR_2 0.1424	0.0603, wR_2 0.1235	0.0393, wR_2 0.0869
Goodness-of-fit	0.976	1.083	1.134	1.144
Maximum, minimum $\Delta\rho$ (e Å^{-3})	0.611, −1.129	1.170, −0.796	2.013, −1.890	1.193, −1.215

[a] Structures were refined on F_0^2: $wR_2 = [\sum[w\,(F_0^2 - F_c^2)^2]/\sum w(F_0^2)^2]^{1/2}$, where $w^{-1} = [\sum(F_0^2) + (aP)^2 + bP]$ and $P = [\max(F_0^2, 0) + 2F_c^2]/3$.

with the SQUEEZE algorithm [32] and the two corresponding structures were refined to convergence. The non-H atoms were refined anisotropically, using weighted full-matrix least-square on F^2. Crystallographic details are summarised in Table 4. Figs. 1, 3–5 were drawn with ORTEP [33] and Fig. 2 with the software MERCURY [34].

3.5. Electrochemistry

Electrochemical measurements are performed on a multipurpose polarograph PA3 interfaced to a Model 4103 XY recorded (both Laboratorní přístroje, Prague) at room temperature using a standard three-electrode cell: rotating (RDE) or stationary platinum disc (1 mm diameter) working electrode, platinum wire auxiliary electrode, and saturated calomel electrode (SCE) reference electrode, the latter separated from the analysed solution by a salt bridge filled with 0.1 M $[Bu_4N][PF_6]$ in *N*,*N*-dimethylformamide. The samples are dissolved in *N*,*N*-dimethylformamide (Aldrich, anhydrous $\geqslant 99.8\%$) to give ca. 5×10^{-4} M concentration of the analyte and 0.1 M $[Bu_4N][PF_6]$ (Fluka, purissimum for electrochemistry). The solutions are purged with argon prior to the measurement and then kept under an argon blanket. Cyclic voltammograms are recorded at stationary platinum disc electrode (scan rates 20–500 mV s^{-1}) while the voltammograms are obtained at RDE (1000–2500 rpm, scan rate 20 mV s^{-1}). Redox potentials are given relative to the reference electrode (SCE); the potential of the ferrocene/ferrocenium couple under the experiment conditions is reproducibly +0.50 V.

3.6. Transfer hydrogenation catalysis

The transfer hydrogenation reactions of acetophenone (0.64 mmol) using **1**–**8** as their hexafluorophosphate salts (6.4 μmol) with formate (3.2 mmol) are carried out in water (5 mL) using a buffer of HCOOH/HCOONa at pH 4 under inert atmosphere. The reaction is quenched by cooling the mixture to 0 °C. The products are extracted by Et_2O and identified (and turnover are determined) by gas chromatography. The pH is monitored using a pH meter (Mettler Toledo InLab® 413) and adjusted using HNO_3 (for pH 3) or NaOH (for pHs 7–9). The initial turnover frequencies are determined for all the catalytic reactions at 30% of conversion for the hydrogenation reaction of the acetophenone to phenylethanol.

Acknowledgement

Financial support of this work by the Swiss National Science Foundation and a generous loan of ruthenium(III) chloride hydrate from the Johnson Matthey Research Centre are gratefully acknowledged. This work is also a part of the long-term research projects of Faculty of Natural Science, Charles University supported by the Ministry of Education of the Czech Republic (project nos. MSM0021620857 and LC06070).

Appendix A. Supplementary material

CCDC 635000, 635001, 635002 and 635003 contain the supplementary crystallographic data for $[\mathbf{3}][PF_6]$, $[\mathbf{5}][PF_6]_2 \cdot (CH_3CN)_3$, $[\mathbf{6}][CF_3SO_3]_2$ and $[\mathbf{7}][PF_6]_2$. These data can be obtained free of charge via http://www.ccdc.cam.ac.uk/conts/retrieving.html, or from the Cambridge Crystallographic Data Centre, 12 Union Road, Cambridge CB2 1EZ, UK; fax: (+44) 1223-336-033; or e-mail: deposit@ccdc.cam.ac.uk. Supplementary data associated with this article can be found, in the online version, at doi:10.1016/j.jorganchem.2007.04.048.

References

[1] W.A. Herrmann, C.W. Kohlpaintner, Angew. Chem., Int. Ed. 32 (1993) 1524–1544.
[2] J. Xiao, X. Wu, A. Zanotti-Gerosa, F. Hancock, Chim. Oggi 23 (2005) 50–55.
[3] S. Ogo, N. Makihara, Y. Watanabe, Organometallics 18 (1999) 5470–5474.
[4] S. Ogo, T. Abura, Y. Watanabe, Organometallics 21 (2002) 2964–2969.
[5] Y. Himeda, N. Onozawa-Komatsuzaki, H. Sugihara, H. Arakawa, K. Kasuga, J. Mol. Catal. A-Chem. 195 (2003) 95–100.
[6] J. Canivet, L. Karmazin-Brelot, G. Süss-Fink, J. Organomet. Chem. 690 (2005) 3202–3211.
[7] T. Abura, S. Ogo, Y. Watanabe, S. Fukuzumi, J. Am. Chem. Soc. 125 (2003) 4149–4154.
[8] S. Ogo, K. Uehara, T. Abura, Y. Watanabe, S. Fukuzumi, Organometallics 23 (2004) 3047–3052.
[9] A. Singh, N. Singh, D.S. Pandey, J. Organomet. Chem. 642 (2002) 48–57.
[10] R. Lalrempuia, M.R. Kollipara, Polyhedron 22 (2003) 3155–3160.
[11] F. Baumann, A. Stange, W. Kaim, Inorg. Chem. Commun. 1 (1998) 305–308.
[12] H. Brunner, A. Köllnberger, T. Burgemeister, M. Zabel, Polyhedron 19 (2000) 1519–1526.
[13] H. Aneetha, P.S. Zacharias, B. Srinivas, G.H. Lee, Y. Wang, Polyhedron 18 (1999) 299–307.
[14] L. Fernholt, C. Romming, S. Samdal, Acta Chem. Scand. A 35 (1981) 707–715.
[15] D.J. Berg, J.M. Boncella, R.A. Andersen, Organometallics 21 (2002) 4622–4631.
[16] (a) M.A. Bennett, A.K. Smith, J. Chem. Soc., Dalton Trans. (1974) 233–241;
(b) M.A.O. Volland, S.M. Hansen, F. Rominger, P. Hofmann, Organometallics 23 (2004) 800–816;
(c) P. Govindaswamy, G. Süss-Fink, B. Therrien, Organometallics 26 (2007) 915–924.
[17] Definitions: E_{pa} and E_{pc} are anodic and cathodic peak potentials, respectively. Similarly, i_{pa} and i_{pc} denote the anodic and cathodic peak currents. i_{lim} is the limiting current and $E_{1/2}$ the half-wave potential in voltammetry at Pt-RDE, v the scan rate, and ω the rotation frequency of the disc electrode.
[18] (a) M. Ladwig, W. Kaim, J. Organomet. Chem. 419 (1991) 233–243;
(b) M. Ladwig, W. Kaim, J. Organomet. Chem. 439 (1992) 79–90;
(c) W. Kaim, R. Reinhardt, M. Sieger, Inorg. Chem. 33 (1994) 4453–4459.
[19] The mechanism suggested by Kaim et al. for $[(arene)MCl(bpym)]^+$ (Ref. [18]) regeneration of $[(arene)MCl(bpym)]^+$ from [(arene)M(bpym)] upon back-oxidation.
[20] W. Kaim, R. Reinhardt, S. Greulich, M. Sieger, A. Klein, J. Fiedler, Collect. Czech. Chem. Commun. 66 (2001) 291–306.

[21] According to ^{1}H NMR spectra, the mono and dinuclear complexes are stable in *N*,*N*-dimethylformamide-d_7 after 12 h at room temperature and even after 1 h at 50 °C.
[22] Reduction of **5** at these potentials is also accompanied with follow-up processes that give rise to minor anodic waves at −0.66 and ca. −0.80 V.
[23] S. Ogo, N. Makihara, Y. Kaneko, Y. Watanabe, Organometallics 20 (2001) 4903–4910.
[24] P. Štěpnička, J. Ludvík, J. Canivet, G. Süss-Fink, Inorg. Chim. Acta 359 (2006) 2369–2374.
[25] A. Gabrielsson, P. van Leeuwen, W. Kaim, Chem. Commun. (2006) 4926–4927.
[26] (a) J.W. Kang, K. Moseley, P.M. Maitlis, J. Am. Chem. Soc. 91 (1969) 5970–5977;
(b) R.G. Ball, W.A.G. Graham, D.M. Heinekey, J.K. Hoyano, A.D. McMaster, B.M. Mattson, S.T. Michel, Inorg. Chem. 29 (1990) 2023–2025;
(c) C. White, A. Yates, P.M. Maitlis, Inorg. Synth. 29 (1992) 228–234.
[27] (a) R.A. Zelonka, M.C. Baird, Can. J. Chem. 50 (1972) 3063–3072;
(b) M.A. Bennett, A.K. Smith, J. Chem. Soc., Dalton Trans. (1974) 233–240.
[28] M.A. Bennett, T.-N. Huang, T.W. Matheson, A.K. Smith, Inorg. Synth. 21 (1982) 74–76.
[29] G.M. Sheldrick, Acta Crystall. A46 (1990) 467–473.
[30] G.M. Sheldrick, SHELXL-97, University of Göttingen, Göttingen, Germany, 1999.
[31] A.L. Spek, J. Appl. Cryst. 36 (2003) 7–13.
[32] P. van der Sluis, A.L. Spek, Acta Crystall., A 46 (1990) 194–201.
[33] L.J. Farrugia, J. Appl. Cryst. 30 (1997) 565.
[34] I.J. Bruno, J.C. Cole, P.R. Edgington, M. Kessler, C.F. Macrae, P. McCabe, J. Pearson, R. Taylor, Acta Crystall. B58 (2002) 389–397.